OBSERVATION OF A POTENTIAL BARRIER CREATED BY ELECTRON CYCLOTRON RESONANCE HEATING IN A MULTIPLE MIRROR PLASMA

by

C. P. Chang, M. A. Lieberman, H. Meuth,
and A. J. Lichtenberg

Memorandum No. UCB/ERL M86/68

11 August 1986

OBSERVATION OF A POTENTIAL BARRIER CREATED BY ELECTRON CYCLOTRON RESONANCE HEATING IN A MULTIPLE MIRROR PLASMA

by

C. P. Chang, M. A. Lieberman, H. Meuth, and A. J. Lichtenberg

Memorandum No. UCB/ERL M86/68

11 August 1986

ELECTRONICS RESEARCH LABORATORY

College of Engineering
University of California, Berkeley
94720

TITLE PAGE

OBSERVATION OF A POTENTIAL BARRIER CREATED BY ELECTRON CYCLOTRON RESONANCE HEATING IN A MULTIPLE MIRROR PLASMA

by

C. P. Chang, M. A. Lieberman, H. Meuth, and A. J. Lichtenberg

Memorandum No. UCB/ERL M86/68

11 August 1986

ELECTRONICS RESEARCH LABORATORY

College of Engineering
University of California, Berkeley
94720

OBSERVATION OF A POTENTIAL BARRIER CREATED BY ELECTRON CYCLOTRON RESONANCE HEATING IN A MULTIPLE MIRROR PLASMA

C. P. Chang, M. A. Lieberman, H. Meuth, and A. J. Lichtenberg

Department of Electrical Engineering and Computer Sciences
and the Electronics Research Laboratory
University of California, Berkeley, CA 94720

Abstract

An electrostatic potential well and mirror-trapped hot electrons are created by high power (250 kW), short pulse (3 μsec) electron cyclotron resonance heating (ECRH) of a plasma in one magnetic mirror cell of the Berkeley Ten Meter Multiple Mirror Experiment. The creation and subsequent decay of potential well is measured by an electron beam, time-of-flight diagnostic. Typically, the barrier rises to -40 volts just after ECRH and decays within 100 μsec. A numerical model of the barrier evolution is developed, and the numerical results along with the experimental observations are presented. Both the numerical results and the experimental observations indicate a correlation between the degree of heating (diamagnetic loop voltage output) and the longevity of the barrier. It is shown that the decay of the barrier is determined mainly by the hot electron escape rate and the hot electron-neutral ionization rate, rather than by the trapping of the passing ions.

I. INTRODUCTION

One promising configuration being investigated for confinement of fusion plasmas is a tandem mirror in which electron cyclotron resonance heating (ECRH) is used in an intermediate mirror cell to create a potential barrier (thermal barrier) to electron flow between outboard anchor cells and the center cell of the device. The electron temperature in an anchor can then be maintained by additional heating to exceed the temperature of center cell electrons. Since the ion confining potential of the anchor with respect to the center cell is proportional to the anchor temperature, strongly enhanced plugging of the center cell ions can be achieved.[1] Experiments on the TMX-U device at the Lawrence Livermore National Laboratory indicate that such a potential barrier and its corresponding enhanced ion confining potential have been achieved.[2]

There are several difficulties to overcome in creating and maintaining a thermal barrier. For example, a trapped particle instability[3] may arise because the communication between the good curvature anchors and the center cell is reduced, thus rendering the stabilizing influence of the anchors less effective. Trapped particle modes have been observed in mirror devices.[4-5] We have recently completed an experimental study of trapped particle modes induced by an ECRH potential barrier in a tandem mirror-like magnetic configuration.[6]

A second problem is to maintain the barrier by pumping out ions which tend to collect there and thus reduce the barrier height. Various schemes such as neutral beam pumping[2] and drift time scale pumping, have been studied. However the ion trapping mechanism and the effectiveness of these schemes are not well characterized. Finally, direct measurements of the actual barrier height are difficult to make because the electron temperature in the barrier region is high and the magnetic field configuration is complicated and often non-axially symmetric. Indirect measurements such as end loss analyzers[8] and

end loss ion spectrometers[9] have been used successfully to measure the barrier potentials. Langmuir probe methods such as differential emissive probes have been used successfully in lower temperature tandem mirror devices.[10]

It is the purpose of this paper to describe observations of a potential barrier produced in a tandem mirror-like magnetic configuration by a single short pulse of ECRH and to describe the transient decay of the barrier after ECRH. The primary potential measurements are made using a modulated electron beam in which the time-of-flight of the beam along a magnetic field line through the ECRH-induced barrier region is determined.[11] The results are compared to a theory of barrier formation and destruction in which hot electron losses, neutral gas ionization, and collisional ion trapping play significant roles.

II. EXPERIMENTAL CONFIGURATION

The measurements are performed in the magnetic mirror system (MMX) shown in Fig. 1. The magnetic field is pulsed, with a rise time of 200 μsec and a decay time of 2 msec. Plasma injected from a Marshall gun source flows along a 225 cm region with a 0.18 T axial magnetic field and through a quadrupole stabilized mirror field at mirror throat T_8, then into three quadrupole stabilized mirror cells with midplanes at M_{78}, M_{67}, and M_{56}. Each cell has length l = 75 cm, midplane field B_0 = 0.18 T, and stable mirror-quadrupole fields having mirror ration R = 3.0 and fan ellipticity $Q \approx 20$.

The 10 cm diameter metal chamber wall of the central cell M_{67}, together with mesh-covered endplates at T_8 and T_7 having openings spaced to fit the elliptical flux surfaces, form a cavity for electron cyclotron resonance heating that does not significantly obstruct the plasma flow. A 3 μsec, 250 kW, 9.0 GHz, rf heating pulse is injected into the cavity at M_{67} which contains an on-axis plasma column. This creates a magnetically confined, hot electron density n_h in the center cell due to ECRH at the two resonance zones, each approximately 6

cm from the mirror throats.

Diagnostics to measure the various plasma parameters include the following: The plasma density in the ECRH cell is measured using an 8 mm, swept-frequency microwave interferometer of conventional design.[12] The interferometer has been calibrated against a commercial phase shifter using rods and slabs of various dielectric constant and radii inserted into the ECRH cavity, and has beam calibrated against a Langmuir probe measurement of the plasma density in M_{67} in the absence of ECRH. The frequency is swept every six microseconds, yielding measurements for plasma densities in the range $10^{11} - 10^{13}$ cm^{-3} on 6 μsec timescales.

The temperature of the "tail" of the hot electron distribution is determined by measuring the x-ray flux in the 1-10 keV range using a cooled, Si(Li) detector with a beryllium window having 47 and 91 percent transmissivity at 1 keV and 2 keV, respectively. The energy resolution of the system is typically 0.4 keV, and the maximum count rate is 500 kHz. Although there is some line radiation observed from high-Z plasma impurities, those with significant amplitudes are sufficiently separated to leave a useful, line-free window between 1.5 and 4 keV to observe the plasma x-ray bremsstrahlung radiation. The preceding measurements are corroborated with a diamagnetic loop which determines the density-energy product of the ECRH plasma just after its formation. The loop and its associated electronics have been calibrated by placing a small solenoid inside the ECRH cell and driving the solenoid current with a square wave generator.

It is necessary to determine the radial plasma profile in order to analyze the interferometer and diamagnetic loop measurements. Arrays of four cylindrical Langmuir probes biased into ion saturation are used to obtain time-resolved radial profile measurements in the central cell midplane in the absence of ECRH, and in the two adjacent cell midplanes with and without ECRH. (Profile

measurements in the central cell midplane in the presence of ECRH could not be performed due to arcing at the probe tipes). We observed little change in radial profile in the adjacent cells with and without ECRH, and little change in the profiles as a function of time.

The transient plasma density and plasma motion in cells M_{56} and M_{78} adjacent to ECRH cell M_{67} are measured using Langmuir probes in the cell midplanes. The probes are biased into ion saturation, with the density inferred from the observed ion current in the usual manner.[13] The transient plasma potentials in the adjacent cell midplanes are measured using high impedance, emissive probes. These same probes, either non emitting or at low emission currents, are also used to measure the floating potentials.

Transient measurements of the cold plasma temperature are required to relate the barrier potential to the temperature and are also used to determine the collisionality regime. To use Langmuir probes as a fast electron temperature diagnostic, the probe bias voltage is swept sinusoidally, with every bias cycle producing an I vs. V plot, ranging from the ion saturation to the electron saturation region. On each plot, the exponential region yields the electron temperature from the relation

$$\ln(I-I_i) = \ln I_e + (V - V_P)/ T_e$$

where I_i and I_e are the ion and electron saturation currents, respectively, and V_P is the plasma potential. A typical sweep frequency of 250 kHz gives a time resolution of 4 μsec. The main complication to the bias sweeping is the finite capacitance from the probe tip to the chamber ground, which is tuned out by a bridge circuit, but only at a single plasma density. Since our plasma density varies with time, some $I-V$ plots have a hysteresis which can be mostly eliminated by computer processing.

For some plasma source and vacuum conditions, the plasma density in the central cell rises sharply just after ECRH. A nude ion gauge is used to monitor the transient pressure rise in the central cell produced by the emission of neutrals from the plasma source and the chamber walls. We interpret some fraction of the plasma density rise after ECRH as being caused by ionization of this transient neutral pressure rise, with the remaining density rise resulting from the potential barrier dynamics, as described subsequently.

To measure the potential barrier in the central cell, an electron beam time-of-flight diagnostic has been developed.[11,6] A schematic of the diagnostic arrangement is shown in Fig. 2. A 100-200 volt, 0.5 mA, 1/8" diameter electron beam is injected in the midplane of cell M_{78}, propagates along the magnetic axis of ECRH cell M_{67}, and is detected in the midplane M_{56} of the following cell. To determine the beam time-of-flight, the beam current is modulated at f = 10 MHz, and the phase delay of the signal received at the collector is measured. To provide high signal-to-noise ratio, a digital, phase-locked loop is used. The beam modulation is synchronized to a 100 MHz transient digitizer, and the received current, after passing through a $Q \approx 7$ tuned amplifier, is digitized to obtain 32 k samples. A sine wave is fitted to each group of fifty consecutive samples, and its amplitude A_j and phase φ_j are determined by a least square error criterion. Ten or twenty consecutive values of $\sin \varphi_j$ (and $\cos \varphi_j$) so determined are then averaged to obtain the mean phase φ and its standard deviation s over the five or ten microsecond sampling interval. It is easily seen that the standard deviation for a set of phases φ_j chosen randomly from the interval $(0,2\pi)$ is $\pi/\sqrt{3}$. However, we typically consider measured phases having $s > 0.6$ as not significant.

The phase $\varphi(x)$ due to an axial potential distribution $V(x)$, with respect to the beam cathode at $x = 0$, is given by

$$\varphi(x) = \omega t(x) = \omega \int_0^x \frac{dx}{v(x)} \tag{1}$$

where

$$v(x) = \left[\frac{2e\ V(x)}{m}\right]^{1/2} ,$$

is the beam velocity. If we assume a simple square well model for the potential, then the phase change $\Delta\varphi$ at $x = 2l$ due to the creation of a negative barrier of magnitude Φ and length l is

$$\Delta\varphi = \frac{\omega l}{v}\left[\left(1 - \frac{\Phi}{V}\right]^{-1/2} - 1\right) . \tag{2}$$

Equation (1) has been verified experimentally by applying a -45 V, 100 μsec pulse to a 2.5 cm diameter ring electrode placed on axis at the midplane of the center cell. The dependence of $\Delta\varphi$ on V in (2) has also been verified over the range from 100 to 200 volts. The time response of the beam diagnostic has been measured by applying a 20 V, peak-to-peak, 25 kHz square wave modulation in series with the cathode voltage. These measurements yield a response time that is less than 5 μsec. The electron beam diagnostic has been used to observe the formation and decay of -40 to -60 volt barriers on 5-10 microsecond timescales.

III. EXPERIMENTAL RESULTS

Due to the irreproducibility of the plasma conditions from discharge to discharge, not every discharge with ECRH produces high-average-energy, well-trapped, heated electrons. A good indication of the effectiveness of the heating is the diamagnetic loop voltage. The experimental observations indicate a strong correlation between the electron beam phase shift and the diamagnetic loop voltage. Therefore, we divide our ECRH discharges into the three categories—low, medium, and high diamagnetic loop voltage. However, all ECRH

discharges do exhibit some common features.

Typical plasma parameters before the initiation of the ECRH pulse are $T_e = T_i \approx 7-8$ eV and $n_{67} \approx 3 \times 10^{11}\text{cm}^{-3}$, with the density decreasing by about a factor of approximately two from cell to cell away from the source. After ECRH, the exponential tail of the hot electron distribution, obtained from pulse height analysis of x-rays, indicates a temperature as high as 1.5 keV. The average energy of the hot electrons, obtained from the diamagnetic loop and microwave interferometer, together with measurements of the radial density profile in adjacent cells, is generally lower, indicating a non-Maxwellian distribution of the hot electrons. After ECRH, the cold electron temperature in midplanes M_{56} and M_{78} jumps to approximately 15 eV and then remains fairly constant for several hundred microseconds. This effect is probably caused by heating due to microwave power leaking out of the cavity. The plasma potential (with respect to the discharge chamber) measured in M_{78} jumps from 6 to 17 volts right after ECRH, then drops to a constant level of about 10 volts in 20 μsec. The general increase of the potential is in qualitative agreement with the temperature increase after ECRH.

Typical ion saturation currents from Langmuir probes in M_{56} and M_{78} are given in Fig. 3a and 3b. A large jump is observed right after the ECRH. The magnitude of the jump implies an increase of the plasma density in addition to the temperature increase, since the temperature increase alone is not enough to account for the magnitude of the jump. The density increase may result from microwave ionization of the background neutrals. The slow wiggles on the density trace (period $\geq$ 40 μs) observed after ECRH indicate a slow plasma motion or rotation, and may be due to an effective "kick" exerted by the microwaves. A typical plasma density at M_{67} from the microwave interferometer is given in Fig. 3c. Qualitatively, the density increases after ECRH and peaks at about 40 μs. Some of the increase in this cell may be caused by hot electron and microwave

ionization of neutrals, as in the adjacent cells, and some of the increase is a result of the potential barrier dynamics.

The phase delay $\Delta\varphi$ [see Eq. (2)] for a discharge with low diamagnetic loop voltage ($V_d \approx 10$ mV) is shown in Fig. 4a. The phase shows a sudden delay right after ECRH of 2 radians that drops back to the original phase ($t < 0$) in about 60 μsec. The x-ray signal vs. time is short (≈ 100 μsec) and weak, indicating that the average energy of heated electrons is much lower than the x-ray window cutoff energy, 1 keV.

The phase delay data for a 40 mV diamagnetic loop voltage discharge is shown in Fig. 4b. A slower decay of the phase than the low V_d case is observed, and the phase returns to its original level in 80 μsec. The x-rays are long-lived, and the average energy of the heated electrons is 770 eV.

The phase delay data for a discharge having an 85 mV diamagnetic loop voltage is shown in Fig. 4c. The phase data indicate a near plateau for 70 μsec, and the phase then drops down sharply afterward. The x-ray signal is strong and long-lived, and the average energy of the heated electrons is 1.4 keV for a density at $t = 0$ of 2.2×10^{11} cm^{-3}.

IV. MODEL OF BARRIER EVOLUTION

We can understand the phase delay data qualitatively using a simple, three cell rate equation model. For ease of notation we use subscript "2" for the ECRH cell M_{67} and subscripts "1" and "3" for the adjacent cells M_{56} and M_{78}. After ECRH, a magnetically confined hot electron population having density n_h suddenly appears, and the cold electron density n_{c2} is suddenly reduced. The potential $-\Phi$ in cell 2 (with respect to cells 1 and 3) follows from the flux balance equation for electrons and ions at each adjacent cell interface required to maintain charge neutrality in the ECRH cell,

$$\frac{n_1 v_e}{4R} e^{-\Phi/T_e} - \frac{n_{c2} v_e}{4R} = \frac{n_1 v_i}{4R} - \frac{n_2 v_i}{4R} e^{-\Phi/T_i} \quad . \tag{3}$$

Here n_1 is the electron (and ion) density in cell 1, $n_2 = n_h + n_{c2}$ is the ion density in cell 2, R is the mirror ratio, T_e and T_i are the cold electron and ion temperature in volts, and v_e and v_i are the average speeds of the electrons and the ions respectively,

$$v_e = (8T_e/\pi m)^{1/2} \quad ,$$

$$v_i = (8T_i/\pi M)^{1/2} \quad .$$

For $T_e = T_i$, we find from (3),

$$\Phi = T_e \ln\left(\frac{n_1\mu + n_2}{n_1 + n_{c2}\mu}\right) \quad , \tag{4}$$

where $\mu = (M/m)^{1/2}$. Just after ECRH, for $n_{c2}\mu \ll n_1 \approx n_2$, we obtain $\Phi \approx 3.75\ T_e$ and a phase delay given by (2).

After ECRH, the cold electron density increases with time as

$$\frac{dn_{c2}}{dt} = \frac{n_1 v_i}{2Rl} - \frac{n_2 v_i}{2Rl} e^{-\Phi/T_i} \tag{5}$$

where we have assumed $n_1 = n_3$. Since $\mu \gg 1$, the barrier potential Φ is roughly proportional to $\ln(n_1/n_{c2})$ and diminishes as n_{c2} increases in time. However, the rate of increase is characterized by the ion velocity v_i. Therefore, according to this simple model, a barrier $\Phi \approx 40$ volts springs up in one electron transit time, typically about 0.5 μs in our experiments, and decays in a few ion transit times ($\approx 40\ \mu$s) due to collisional ion trapping. Note that there is a non-zero asymptotic value of the barrier depth which is obtained by setting (5) equal to zero and using (4).

$$\Phi_{asym} \approx 0.48\ T_e\ .$$

This value results because the ion density in cell 2 is always higher than that in an adjacent cell due to the trapped hot electrons.

Although the preceding description of barrier evolution agrees qualitatively with measurements, several additional features have been incorporated into the model in order to make a quantitative comparison. First, for the parameters of the experiment, the ion flux entering cell 2 is not completely collisionally trapped. We let

$$\chi_i = 1 - \exp(-l/\lambda_i^*)$$

be the fraction of the incoming ion flux that is trapped, where $\lambda_i^* = \lambda_i / R$ is the effective mean free path for scattering through a loss cone angle $\sin^{-1}(R^{-1/2})$ and λ_i is the ion collisional mean free path, which is given by

$$\lambda_i(\mathrm{cm}) \approx 8 \times 10^{11}\ \frac{\varepsilon_i^2(\mathrm{eV})}{n(\mathrm{cm}^{-3})\ln\Lambda}\ ,$$

where $\varepsilon_i = \Phi + \frac{3}{2} T_i$ and $\ln \Lambda \approx 15$ is the Coulomb logarithm.[14] Since $\Phi \approx 40$ V, the ion mean free path can be longer than the cell length, and the ion trapping fraction can be much less than unity. Thus most ions are not trapped while traversing the ECRH cell; instead they are mostly *passing* ions.

A second feature is the loss of hot electrons during barrier formation and decay. This loss modifies the electron flux balance at the adjacent cell interfaces, and is particularly important for discharges with low diamagnetic loop voltages. Another addition to the model is ionization of neutral gas in the ECRH cell by hot electrons. A final consideration is that we have used *symmetric* adjacent cells--the plasma parameters of cell 1 are identical to these of cell 3. In reality, the plasma density is quite different from cell to cell. However, the plasma tem-

perature and the plasma potential we have measured are roughly the same in cell 1 and cell 3. It seems that constant plasma potential contradicts large cell-to-cell density variation, as predicted from the Boltzmann factor; i.e., $V_3 - V_1 \approx T_e \ln(n_3/n_1)$. However, due to multiple mirror action in the long machine, electron losses through the ends are significantly inhibited and radial ion losses are comparable to axial electron losses, thus clamping $V_3 \approx V_1$ near chamber ground.[15] These lower potentials are observed on the emissive probe data in the adjacent cells both before and after ECRH. This poses a constraint on the barrier modeling. If we comply with the fact of unsymmetric densities and use the actual densities of the adjacent cells to calculate the barrier depth at the adjacent cell interfaces, the barrier depth at each interface will not be the same. In other words, this simple approach can not properly simulate the barrier evolution in the actual experiments. To simulate the measured scenario, we keep the symmetric property in our model and use the average density measured in the two adjacent cells as the (single) adjacent cell density.

From the preceding considerations, we therefore write, in place of (3) and (5), the modified flux balance and rate equation

$$\frac{n_1 v_e}{4R} e^{-\Phi/T_e} - \frac{n_{c2} v_e}{4R} - \frac{n_h l}{2\tau_h} = \chi_i \frac{n_1 v_i}{4R} - \frac{n_{i2}^t v_i}{4R} e^{-\Phi/T_i} \tag{6}$$

and

$$\frac{dn_{c2}}{dt} = \frac{n_h}{\tau_h} + \chi_i \frac{n_1 v_i}{2R} - \frac{n_{i2}^t v_i}{2R} e^{-\Phi/T_i} + \nu_h^i n_h \ , \tag{7}$$

where

$$\frac{dn_h}{dt} = -\frac{n_h}{\tau_h} \tag{8}$$

describes the decay of the hot electrons and where n_{i2}^t denotes the trapped ion density in cell 2, τ_h is the hot electron collisional scattering time, and ν_h^i is the ionization rate. We approximate[14]

$$\tau_h^{-1} = 1.5 \times 10^{-5} \frac{n_{i2}+2n_h}{T_h^{3/2}} \text{ sec}^{-1} \tag{9}$$

and[16]

$$\upsilon_h^i = \frac{10^{-5}\sqrt{Z}n_0}{E_i^{3/2}(6+Z)} e^{-1/Z} \text{ cm}^3/\text{sec} \tag{10}$$

where $Z = T_h/E_i$, E_i is the ionization potential and n_0 is the neutral density. In (9) and (10) densities are in cm^{-3} and energies in eV. The trapped ion density is given by

$$n_{i2}^t = n_{c2} + n_h - n_{i2}^p \ , \tag{11}$$

where

$$n_{i2}^p = \chi_i \frac{n_2 \upsilon_i}{2R\langle \upsilon_i \rangle} \tag{12}$$

is the passing ion density in cell 2 and

$$\langle \upsilon_i \rangle = [e(T_i+2\Phi)/M]^{1/2} \tag{13}$$

is the average parallel traversing velocity of the passing ions in the ECRH cell. Finally we need the evolution equation for the hot electron temperature,

$$n_h \frac{dT_h}{dt} = -\psi_{hc} n_{c2} - \upsilon_h^i n_h E_0 \ , \tag{14}$$

where ψ_{hc} is the energy transfer rate through collisions from hot to cold electrons and has the form[14]

$$\psi_{hc} = 9 \times 10^{-5} n_h \frac{T_h - T_c}{(T_h+T_c)^{3/2}} \text{ eV}/\mu\text{s}$$

We have numerically integrated the rate equations (7), (8), and (14) along with the flux balance condition (6). Since χ_i and n_{i2}^p are functions of Φ, the equations have to be iterated, given guesses, to obtain Φ, n_{i2}^t and χ_i for every time

step. Further details of the numerical model are given in reference 15. To initialize the simulation, we have made a few approximations which do not alter the physical picture. We assume the ECRH is completed instantaneously. In the experiments, the microwave pulse is about 3 μs long; however, we are not interested in the heating process. Therefore, we just "turn on" a heated electron population at t = 0 in the simulation. Another approximation has to do with the initial transient of the barrier evolution, which is due to the finite traversing time $\tau_i^t = l/\langle v_i \rangle$ of the passing ions. Before the ion flux entering the ECRH cell at $t = 0$ travels one cell length, the passing ions do not exist. Therefore, we can not simulate the transient in a simple manner. Instead, we account for its effect as follows: For $t < \tau_i^t$ which is about 7 μs, (7) can be approximated, for Φ large, as

$$\frac{dn_{c2}}{dt} = \frac{n_1 v_i}{2Rl} + \frac{n_h}{\tau_h} + v_h^i n_h \quad . \tag{15}$$

From (15) the cold electron density at $t = \tau_i^t$ in cell 2, assumed to be zero right after the ECRH, is

$$n_{c2}^+ = \frac{n_1 v_i}{2R\langle v_i \rangle} + \frac{n_h l}{\tau_h \langle v_i \rangle} + v_h^i n_h \frac{l}{\langle v_i \rangle} \quad . \tag{16}$$

Then we use the value of n_{c2}^+ as the cold electron density at the start of the numerical simulation. Note that the aforementioned approximations make the starting time of the simulation about 10 μs later than $t = 0$ in the experimental data (the trigger of the magnetron). To distinguish this difference, we label the time scale of the experimental data as t and the time scale of the simulation output as t^*, with $t \approx t^* + 10$ μs.

V. COMPARISON OF MODEL WITH EXPERIMENT

Figure 4a shows the phase delay for a discharge with a low diamagnetic loop voltage (≈ 10 mV). For the simulation, we use a generic density trace shown in Fig. 5 as our adjacent cell density, which features a mild density jump at $t^* = 0$ and a smooth decay. The other parameters used at $t^* = 0$ are: $n_{i2} = 1 \times 10^{11}$ cm^{-3}, $T_h = 200$ eV, $p = 3 \times 10^{-6}$ torr, $T_e = 15$ eV, and $T_i = 7.5$ eV. The simulation results are given in Figs. 6 and 7. Figure 6 contains four plots: the cold electron density (n_{c2}), the ion trapping fraction (χ_i), the heated electron density (n_w), and the total ion density (n_{i2}) versus time. From the figure, χ_i is very low at $t^* = 0$, and the main mechanisms for the cold electron build-up are hot electron ionization of neutrals and hot electrons scattering out of the ECRH cell. At this hot electron temperature, 200 eV, the cold electrons build up very fast and the barrier decays away by $t^* = 55$ μs (Fig. 7). The barrier depth obtained from the measured phase delay in Fig. 4a, assuming a constant cold electron temperature of 15 eV, is shown in Fig. 7 for comparison with the model results. The barrier depth from the simulation is in good agreement with the observed depth.

The phase delay data for a 40 mV diamagnetic loop voltage discharge are shown in Fig. 4b. For the simulation we use most of the aforementioned parameters, except we choose T_h to be 500 eV and n_{i2} to be 2.4×10^{11} cm^{-3}. Figure 8 shows, in comparison to Fig. 6, a slower rise of the cold electron density n_{c2} due to a much lower loss rate of the hot electrons, which varies as $T_h^{-3/2}$. The barrier depth from the model and from the experiment shown in Fig. 9 displays slower changes compared to the low diamagnetic loop voltage case (Fig. 7). The simulation and observations are in good agreement.

Figure 4c displays the phase delay data for a discharge with an 85 mV diamagnetic loop voltage. The density is 2.2×10^{11} cm^{-3} and the hot electron

temperature is T_h = 1.1 keV. The results are given in Figs. 10 and 11. The trapping fraction χ_i is very low during the entire simulation, and n_{c2} increases mainly due to the hot electron-neutral ionization and the hot electron loss. The barrier depth is significant at t^* = 100 μs. The resulting barrier depth (Fig. 11) does not quantitatively reproduce the observed plateau and sharp drop-off. However, the simulation does indicate a longer lasting barrier compared to the low and medium diamagnetic loop voltage cases.

VI. DISCUSSION AND CONCLUSIONS

The phase delay and temperature results from the simulations are generally in good agreement with the experimental observations. The main mechanisms for the barrier decays are hot electron-neutral ionization and hot electron loss. Ion trapping is not important when the barrier depth is large. The cold electron temperature jump from 7.5 eV before ECRH to 15 eV after ECRH helps to explain the larger barrier depth observed. The effectiveness of the heating (diamagnetic loop voltage) sets the range for the hot electron temperature, which in turn dictates the ionization rate and the hot electron loss rate. Thus, the longevity of the phase delays should be strongly dependent on the diamagnetic loop voltage, which fact is demonstrated by both the simulation and the experimental observations. The discrepancy in the high diamagnetic loop voltage case implies that some mechanism not considered in the numerical model is important in accelerating the barrier decay later in the barrier evolution. One possible mechanism is the arrival of neutrals from the wall of the ECRH cell. Neutrals created by the ECRH microwave pulse at the wall can migrate into the bulk of the heated electrons at a speed of about 1 mm per microsecond. Since the chamber radius is about 5 cm, it will take 50 μs for these neutrals to reach the center and get ionized. These extra ionizations will accelerate the cold electron buildup and the barrier decay. This effect has not

been studied in the numerical model due to lack of proper measurements. However, the density from the microwave interferometer (Fig. 3c) may qualitatively give an indication of the arrival of neutrals from the wall. Therefore, we also simulate a case with a time-varying neutral pressure, shown in Fig. 12a. Using the same parameters as the high diamagnetic loop voltage case, we obtain a phase delay result much closer to the experimental observation in Fig. 4c.

In conclusion, the electron beam, phase sensitive, time-of-flight diagnostic has successfully provided a direct, time-resolved measurement of the thermal barrier evolution in our ECRH experiments, and the experimental observations are quantitatively consistent with our numerical model.

ACKNOWLEDGEMENTS

This work was supported by the Department of Energy Contract No. DE-AT03-76ET53059. The authors would like to thank B. Archer, N. M. P. Benjamin, and J. C. Fernandez for their assistance and valuable guidance.

REFERENCES

[1]D. E. Baldwin and B. G. Logan, Phys. Rev. Lett. **43**, 1318 (1979).

[2]D. P. Grubb, S. L. Allen, T A. Casper, J. F. Clauser, F. H. Coensgen, D. L. Correll, W. F. Cummins, C. C. Damm, J. H. Foote, R. K. Goodman, D. N. Hill, E. B. Hooper, Jr., R. S. Hornady, A. L. Hunt, R. G. Kerr, G. W. Leppelmeir, J. Marilleau, J. M. Moller, A. W. Molvik, W. E. Nexsen, W. L. Pickles, G. D. Porter, P. Poulsen, E. H. Silver, T. C. Simonen, B. W. Stallard, W. C. Turner, W. L. Hsu, T. L. Yu, J. D. Barter, T. Christensen, G. Dimonte, T. W. Romesser, R. F. Ellis, R. A. James, C. J. Lasnier, L. V. Berzins, M. R. Carter, C. A. Clower, B. H. Failor, S. Falabella, M. Flammer, and T. Nash, Phys. Rev. Lett. **53**, 783 (1984).

[3]H. L. Berk, M. N. Rosenbluth, H. V. Wong, T. M. Antonsen, and D. E. Baldwin, Sov.

J. Plasma Phys. **9**, 108 (1983).

[4]S. C. Prager, T. C. Marshall, and A. K. Sen, Plasma Phys. **17**, 785 (1975).

[5]G. A. Navratil, A. K. Sen, and J. Slough, Phys. Fluids, **26**, 1044 (1983).

[6]J. C. Fernandez, C. P. Chang, A. J. Lichtenberg, and M. A. Lieberman, Phys. Fluids **29**, 1208 (1986).

[7]D. E. Baldwin, Bull. Am. Phys. Soc. **26**, 102 (1981); Y. J. Chen, J. A. Byers, and D. E. Baldwin, Bull. Am. Phys. Soc. **29**, 1228 (1985).

[8]D. P. Grubb, "Plsma Potential Formation and Measurement in TMX-U and MFTF-B," Fifth Topical Conf. on High Temperature Plasma Diagnostics, American Physical Society, Lake Tahoe, CA, Sept. 16-20, 1984.

[9]J. H. Foote, Bull. Am. Phys. Soc. **30**, 1581 (1986).

[10]E. Y. Wang, N. Hershkowitz, T. Intrator, J. R. Ferron, J. Pew, B. Nelson, and R. Goulding, Bull. Am. Phys. Soc. **30**, 1491 (1985).

[11]C. P. Chang, J. C. Fernandez, A. J. Lichtenberg, M. A. Lieberman, and H. Meuth, Bull. Am. Phys. Soc., **29**, 1227 (1984).

[12]G. Lisitano, Rev. Sci. Instrum. **36**, 364 (1965).

[13]J. G. LaFromboise in *Rarified Gas Dynamics* edited by J. H. de Leeuw (Academic Press, New York, 1966) Vol. 2, pp. 22-44.

[14]D. Book, NRL Plasma Formulary, Revised, (Naval Res. Lab., Washington, DC, 1983).

[15]C. P. Chang, "Electron Beam Phase Sensitive Measurements of Electrostatic Potential Barrier Produced by ECRH on the Ten Meter Multiple Mirror

Experiment," PhD thesis, College of Engineering, University of California, Berkeley (1985), Appendix E.

[16]R. McWhirter, *Spectral Intensities*, in Plasma Diagnostic Techniques, R. Huddlestone and S. Leonard, editors (Academic Press, NY, NY, 1965).

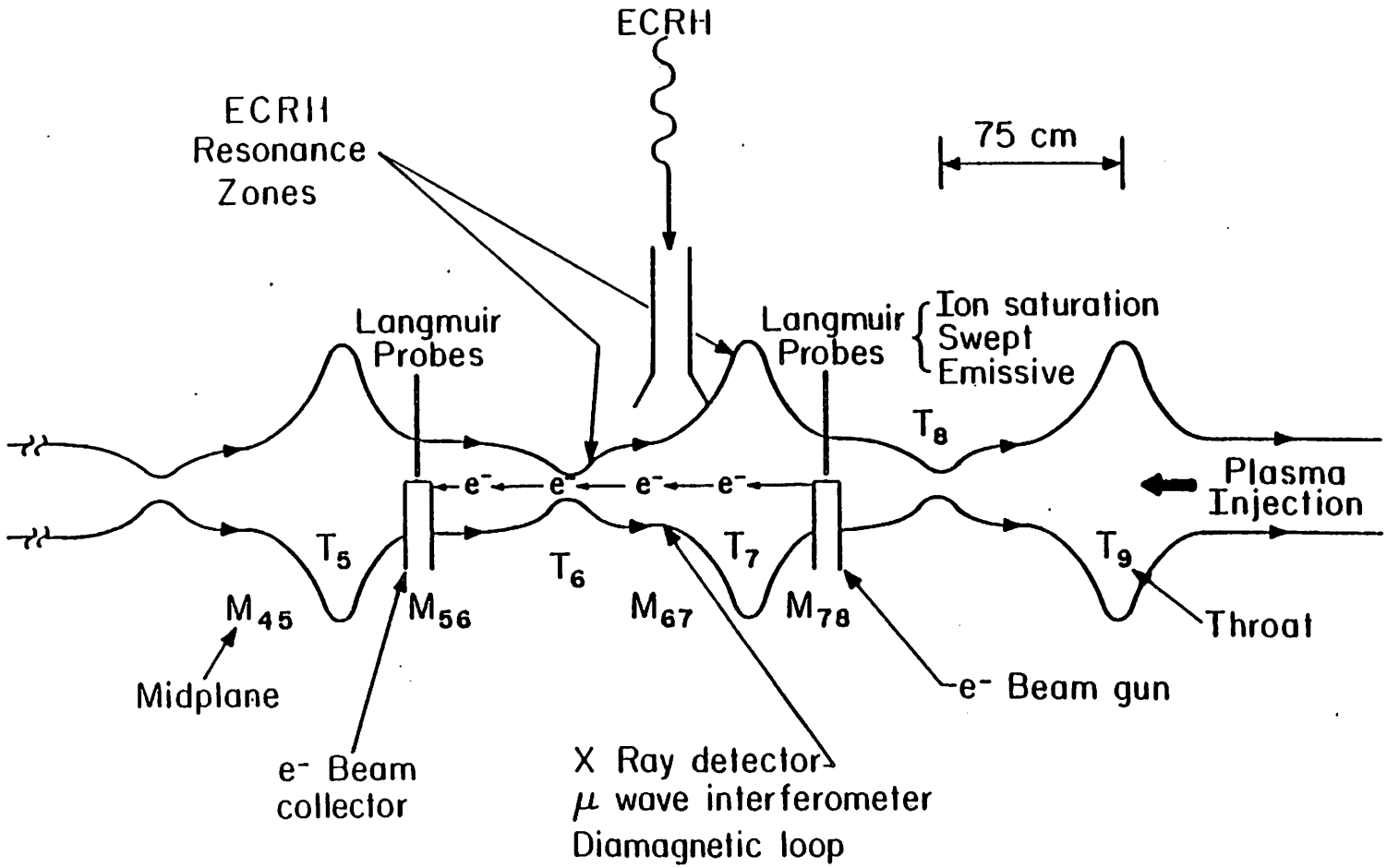

Figure 1. Experimental configuration, including a schematic (not to scale) of two magnetic field lines 180 degrees apart. The mirror midplanes (M) and throats (T) are indicated.

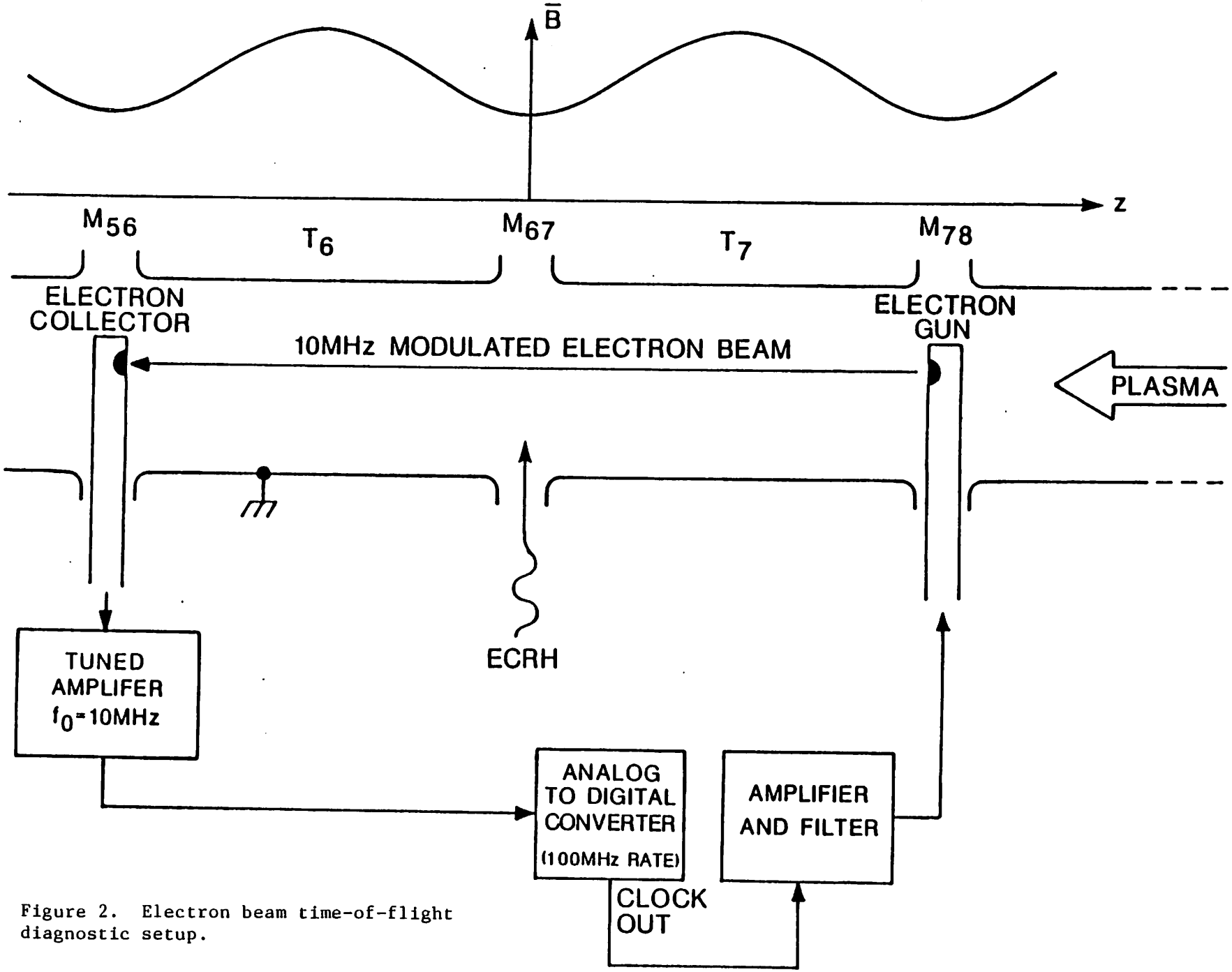

Figure 2. Electron beam time-of-flight diagnostic setup.

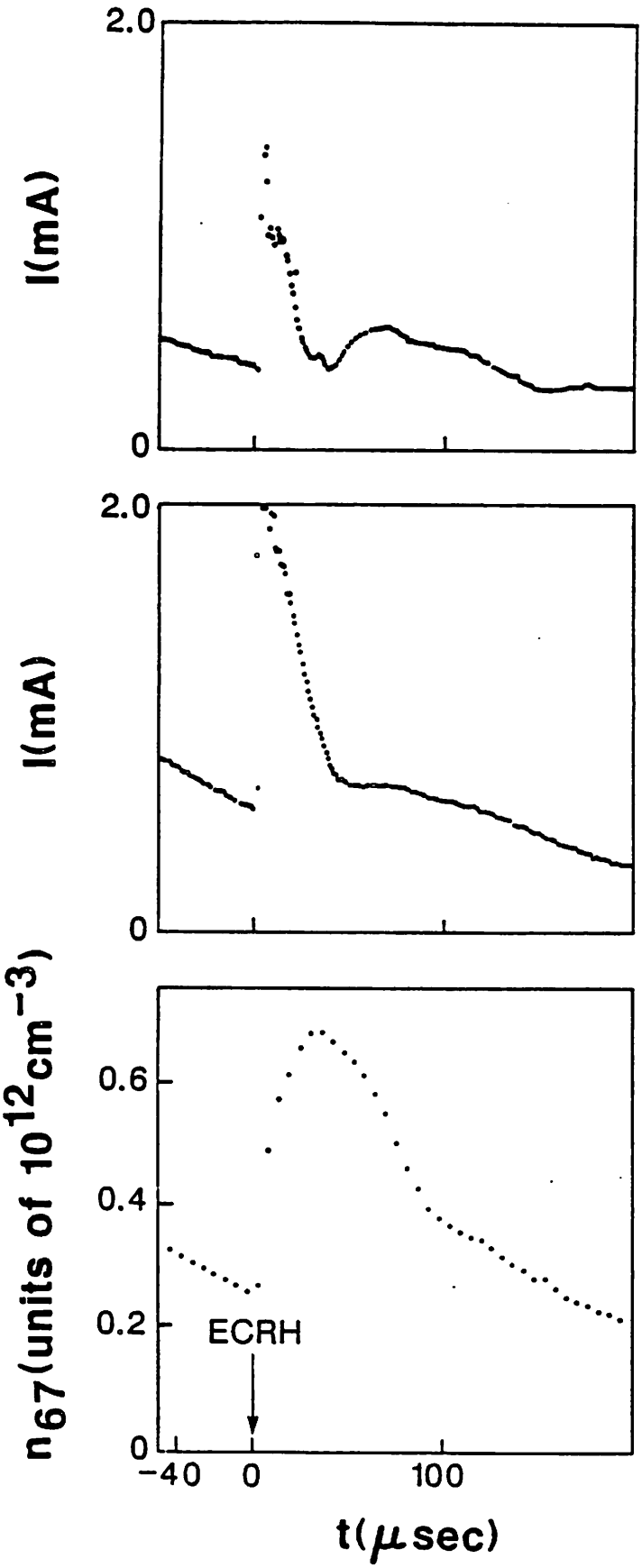

Figure 3. Density vs time with ECRH; (a) and (b) give Langmuir probe ion saturation currents in M_{56} and M_{78} respectively; (c) gives density measured by microwave interferometry in M_{67}.

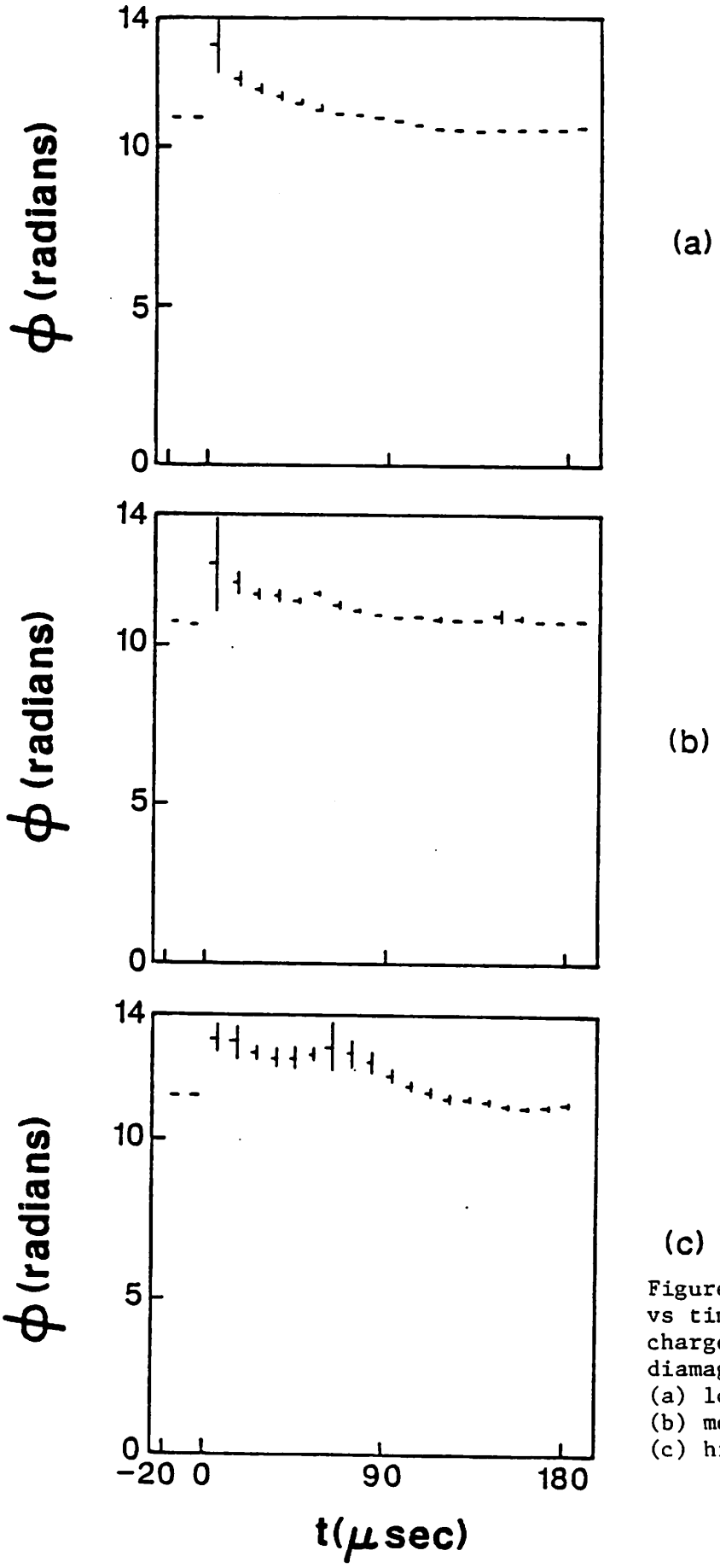

Figure 4. Phase delay ϕ vs time t for three discharges with different diamagnetic loop voltages: (a) low voltage V_d = 10 mV; (b) medium voltage V_d = 40 mV; (c) high voltage V_d = 85 mV.

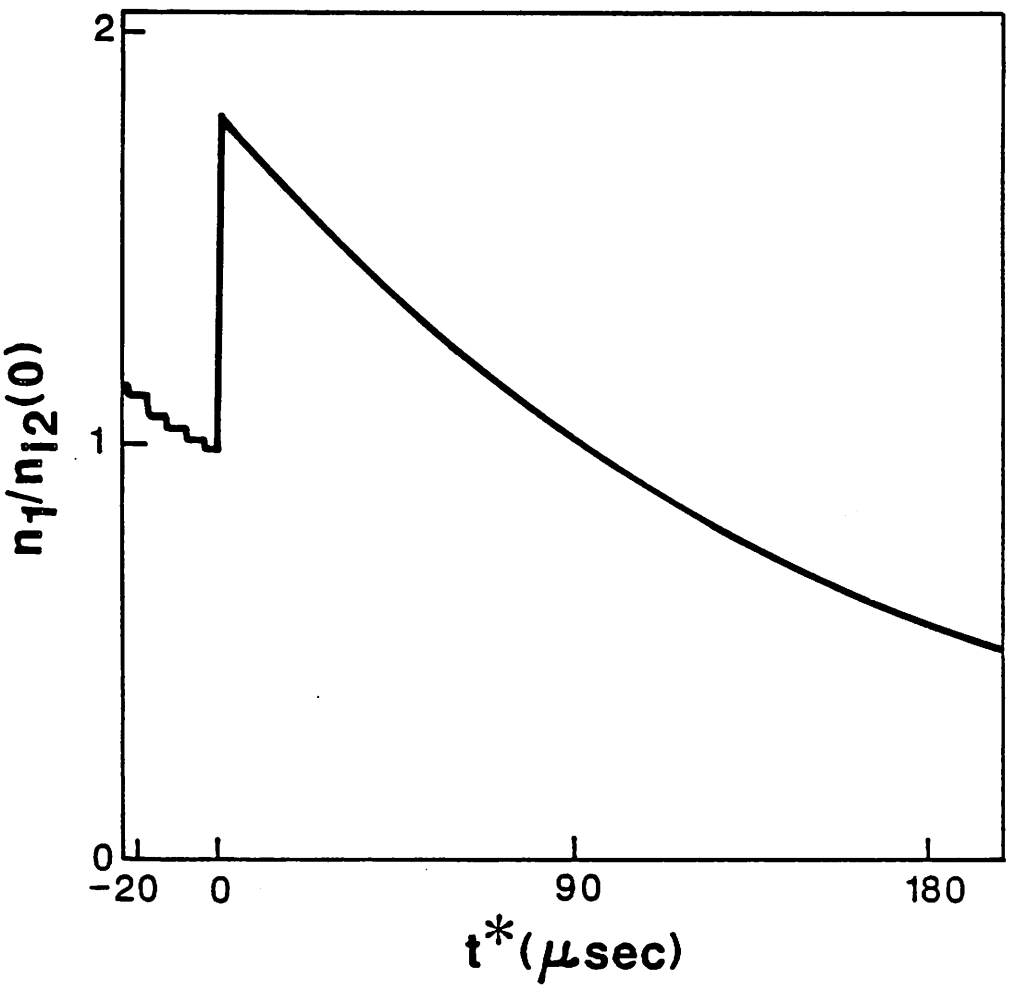

Figure 5. The symmetrized adjacent cell density input n_1 vs t^*.

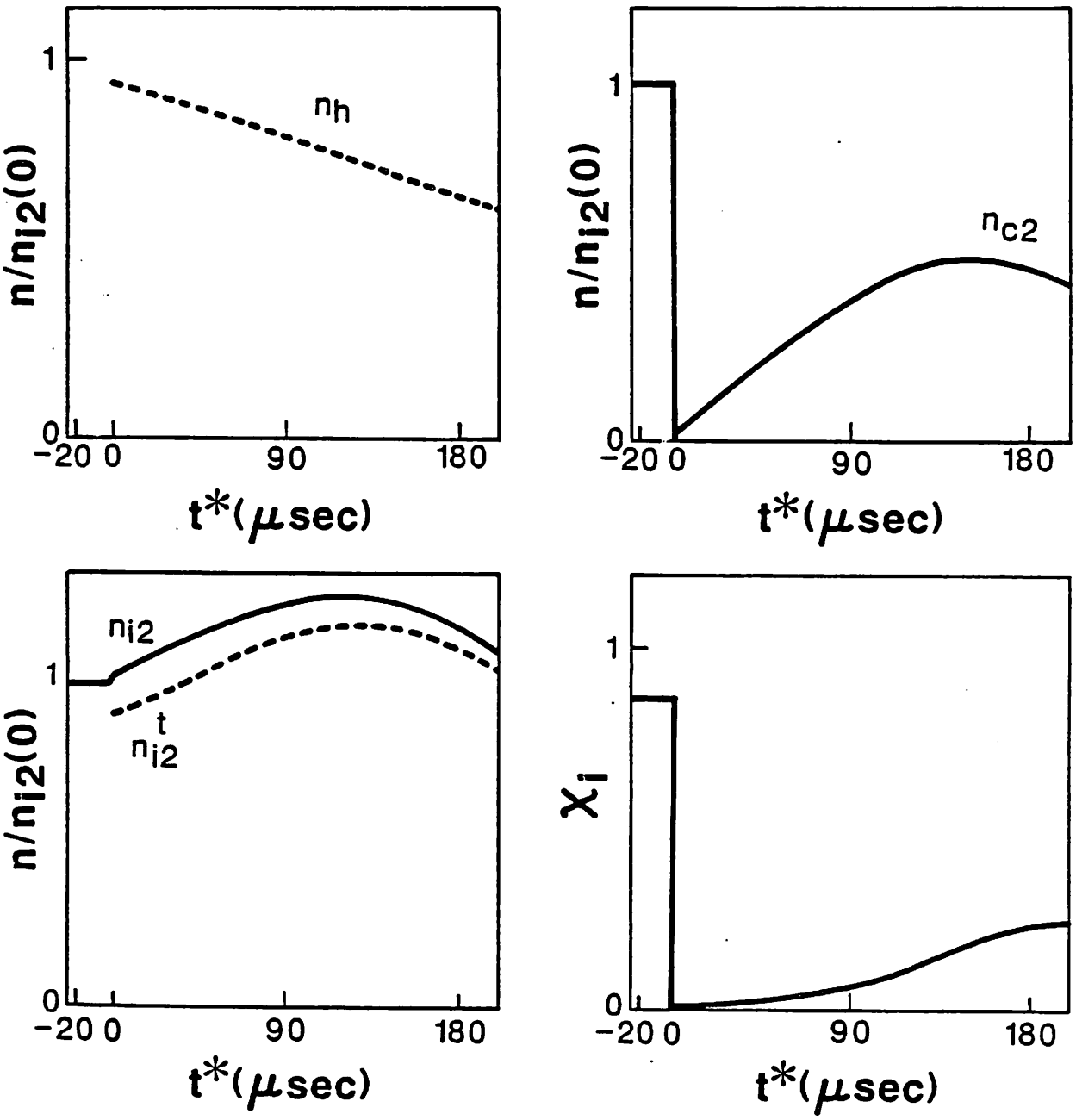

Figure 6. Electron densities n_h and n_{c2}, ion densities n_{i2} and n_{i2}^t, and ion trapping fraction χ_i vs time t^*, from the simulation for a low diamagnetic loop voltage discharge.

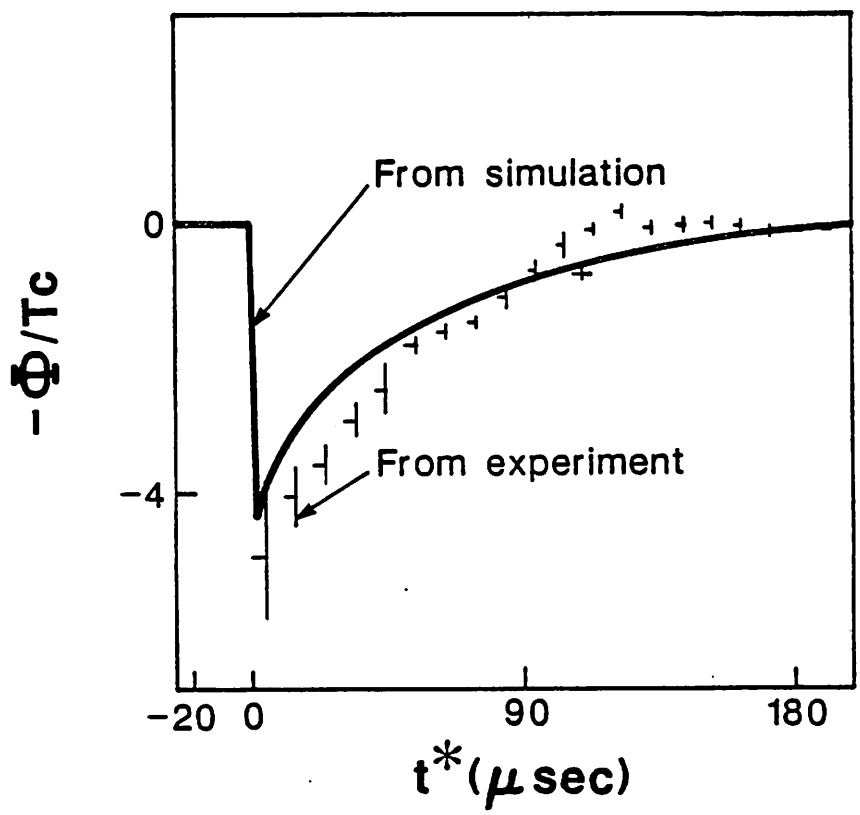

Figure 7. Barrier depth Φ/T_e vs time t^* for a low diamagnetic loop voltage discharge. The solid line is the simulation result and the crosses give the measured result, with the height of each cross indicating the standard deviation of the phase delay measurement.

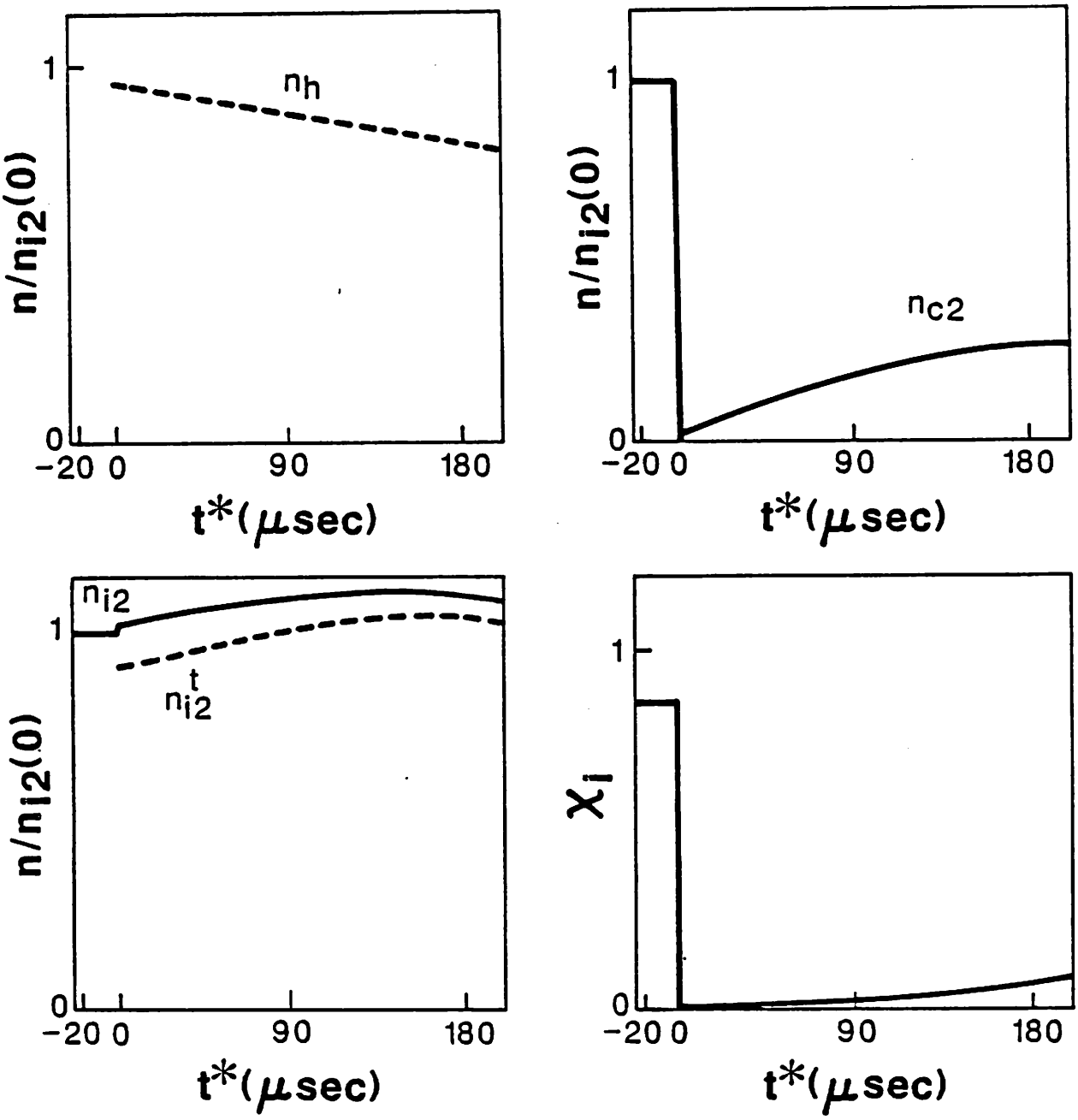

Figure 8. Electron densities n_h and n_{c2}, ion densities n_{i2} and n_{i2}^t, and ion trapping fraction χ_i vs time t^*, from the simulation for a medium diamagnetic loop voltage discharge.

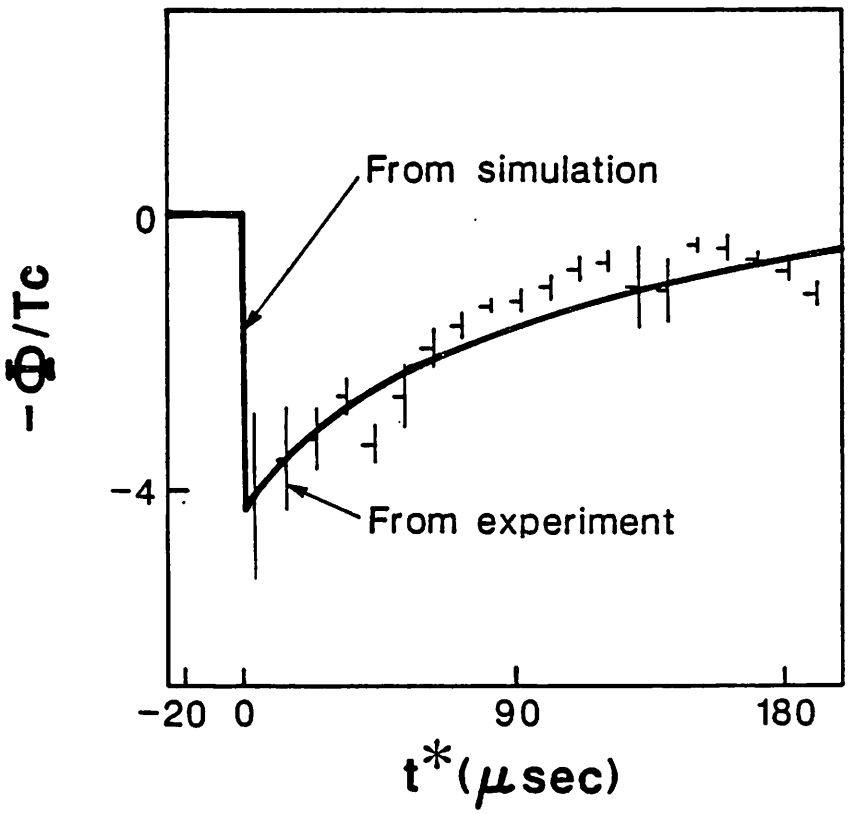

Figure 9. Barrier depth Φ/T_e vs time t^* for a medium diamagnetic loop voltage discharge. The solid line is the simulation result and the crosses give the measured result, with the height of each cross indicating the standard deviation of the phase delay measurement.

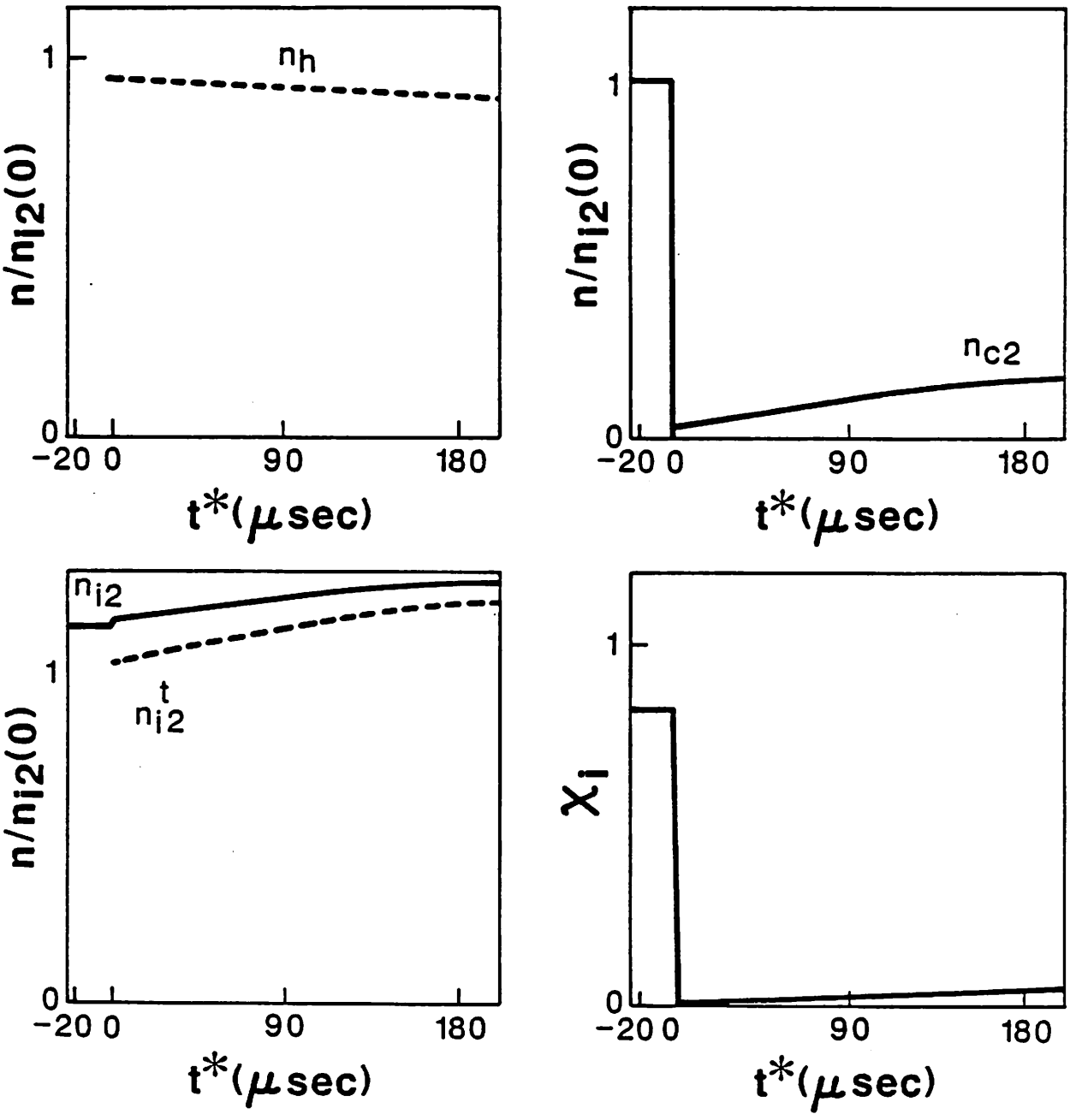

Figure 10. Electron densities n_h and n_{c2}, ion densities n_{i2} and n_{i2}^t, and ion trapping fraction χ_i vs time t^*, from the simulation for a high diamagnetic loop voltage discharge.

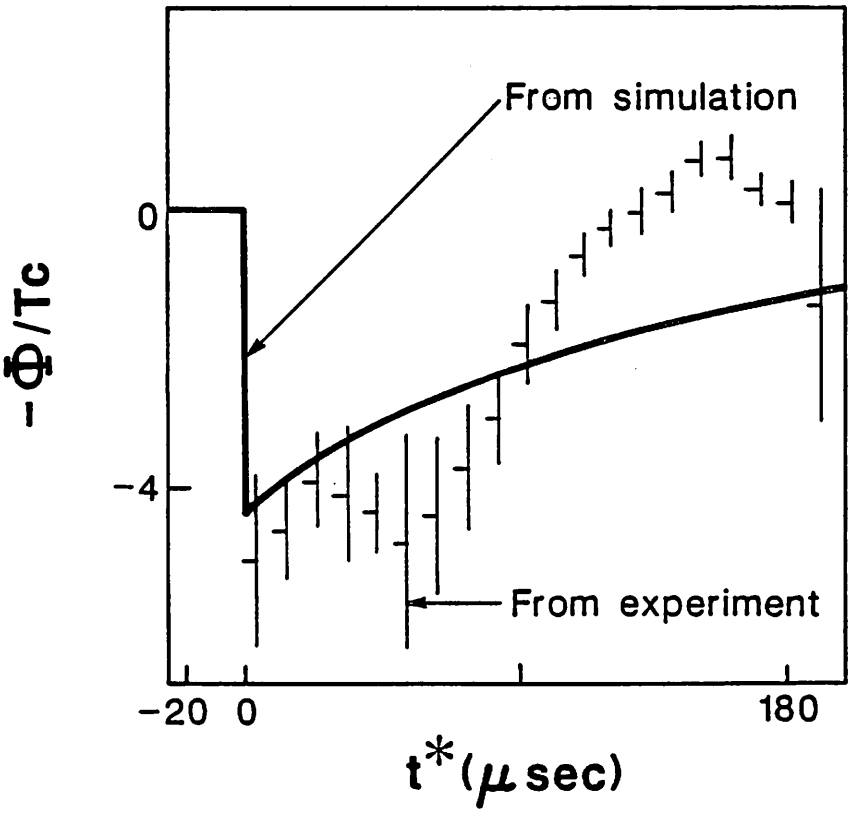

Figure 11. Barrier depth Φ/T_e vs time t^* for a high diamagnetic loop voltage discharge. The solid line is the simulation result and the crosses give the measured result, with the height of each cross indicating the standard deviation of the phase delay measurement.

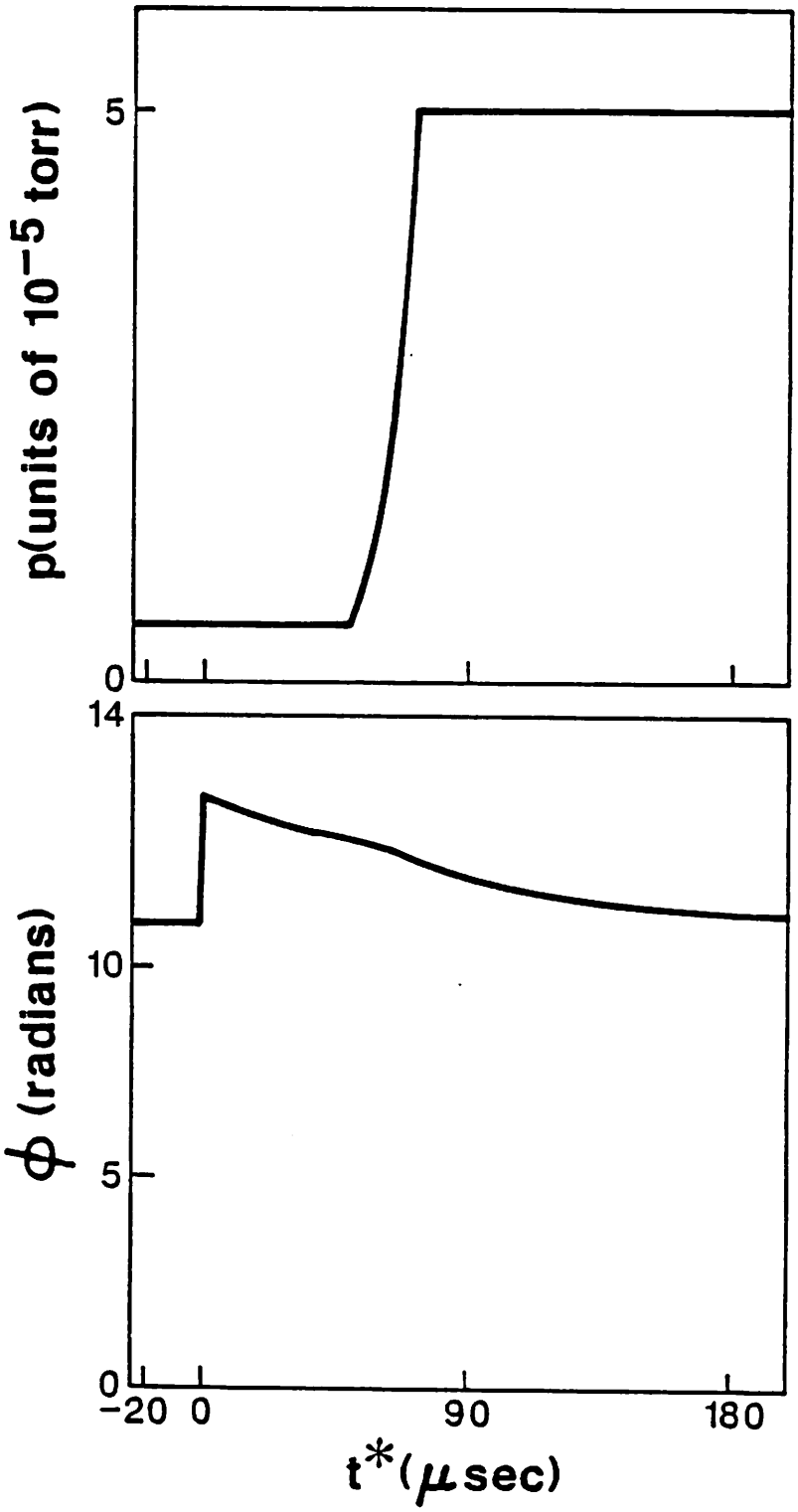

Figure 12. Simulation with time varying pressure, showing (a) pressure vs time and (b) phase delay vs time for a high diamagnetic loop voltage discharge.